Carbon Isotope Separation and Molecular Formation in Laser-Induced Plasmas by Laser Ablation Molecular Isotopic Spectrometry

ARTICLE *in* ANALYTICAL CHEMISTRY · FEBRUARY 2013

Impact Factor: 5.64 · DOI: 10.1021/ac303524d · Source: PubMed

5 AUTHORS, INCLUDING:

Meirong Dong
University of California, Berkeley
15 PUBLICATIONS **165** CITATIONS
SEE PROFILE

Xianglei Mao
Lawrence Berkeley National Laboratory
167 PUBLICATIONS **4,682** CITATIONS
SEE PROFILE

Jhanis J Gonzalez
Lawrence Berkeley National Laboratory
51 PUBLICATIONS **1,109** CITATIONS
SEE PROFILE

Jidong Lu
South China University of Technology
38 PUBLICATIONS **499** CITATIONS
SEE PROFILE

analytical chemistry

Article

pubs.acs.org/ac

Carbon Isotope Separation and Molecular Formation in Laser-Induced Plasmas by Laser Ablation Molecular Isotopic Spectrometry

Meirong Dong,[†,‡] Xianglei Mao,[‡] Jhanis J. Gonzalez,[‡] Jidong Lu,[†] and Richard E. Russo*[,‡]

[†]School of Electric Power, South China University of Technology, Guangzhou, Guangdong 510640, China

[‡]Lawrence Berkeley National Laboratory, University of California, Berkeley, California 94720, United States

ABSTRACT: Laser ablation molecular isotopic spectrometry (LAMIS) recently was reported for rapid isotopic analysis by measuring molecular emission from laser-induced plasmas at atmospheric pressure. This research utilized the LAMIS approach to study C_2 molecular formation from laser ablation of carbon isotopic samples in a neon gas environment at 0.1 MPa. The isotopic shift for the Swan system of the C_2 $\Delta\nu = 1$ band was chosen for carbon isotope analysis. Temporal and spatial resolved measurements of $^{12}C_2$, $^{12}C^{13}C$, and $^{13}C_2$ show that C_2 forms from recombination reactions in the plasma. A theoretical simulation was used to determine the temperature from the molecular bands and to extract the isotopic ratio of $^{12}C/^{13}C$ derived from $^{12}C_2$, $^{12}C^{13}C$, and $^{13}C_2$. Our data show that the ratio of $^{12}C/^{13}C$ varies with time after the laser pulse and with distance above the sample. $^{12}C/^{13}C$ deviates from the nominal ratio (2:1) at early times and closest to the sample surface. These measurements provide understanding of the chemical processes in the laser plasma and analytical improvement using LAMIS.

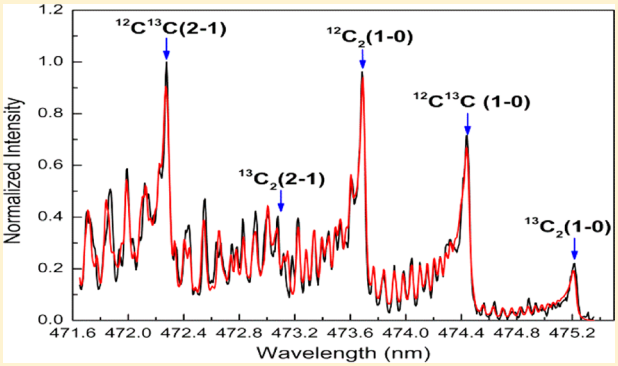

Isotope measurements in laser plasmas are of current interest for both fundamental understanding of plasma properties and for applications. Isotope separation in laser-induced plasmas has been reported under different ablation conditions and using different methods of detection.[1−5] Several studies showed isotope separation directly in the laser plume and by depositing films.[6−8] Mechanisms for isotope fractionation are under investigation and not well established. Atomic emission from laser-induced plasmas has been demonstrated as an approach for the analysis of isotope ratios, with studies at reduced and atmospheric pressure.[9−12] Laser ablation molecular isotopic spectrometry (LAMIS) is a promising approach for real-time isotopic analysis of samples at ambient pressure.[13−16] The technology exploits the measurement of optical spectra from molecular species that are produced during plasma expansion into air. Optical isotope shifts in molecular spectra are significantly larger than those in atomic spectra; differences in isotopic masses have only a small effect on electronic transitions (atoms) but appreciably affect the vibrational and rotational energy levels in molecules.[13] Large shifts in the isotope molecular bands of several elements in laser ablation plasmas were presented; boron and strontium isotopes were demonstrated using the LAMIS technology.[13−15]

Carbon is one of the most abundant elements in geological and natural materials, and it is present in all known life forms. There are two stable isotopes, ^{12}C and ^{13}C. The study of ^{13}C is related with research areas including climate change,[17] coal combustion,[18] human diet,[19] plants,[20] and others.[21,22] Carbon molecular emission has been measured in sources like flames, electric arcs, and furnaces, and it has also been detected in a number of astrophysical environments including the sun, interstellar gas clouds, late-type stars, and comets;[23] there is abundant literature of its spectroscopy.[24−26] Pesic et al.[27] observed the swan bands of $^{13}C_2$ and $^{12}C^{13}C$ in a low pressure hollow discharge spectrum and derived the molecular constants for several bands. A series of $^{12}C_2$, $^{13}C_2$, and $^{12}C^{13}C$ were made by Amiot and co-workers; Amiot and Verge[28,29] recorded the (0−0) band of the Swan system of $^{12}C_2$, $^{12}C^{13}C$, and $^{13}C_2$ by Fourier spectroscopy and made a complete analysis for the $a^3\Pi$ and $d^3\Pi$ ($v = 0$) levels. Perturbations were observed in the $d^3\Pi_g$ ($v = 0$) level, and their origins were discussed. The (0−0) and (1−0) bands of the Phillips system and the (0−0) band of the Ballik-Ramsay system of $^{13}C_2$ and $^{12}C^{13}C$ were observed and analyzed using a microwave electromagnetic field with the high accuracy of the Fourier transform interferometer. Curtis and Sarre[30] analyzed the nuclear hyperfine structure of $^{13}C_2$ by laser-induced fluorescence to yield Fermi-contact parameters.

Optical emission in the laser ablation plasma, known as laser-induced breakdown spectroscopy (LIBS), offers an ideal characteristic for real-time elemental analysis and in situ plasma characterization at atmospheric pressure.[31−36] In a number of previous studies, carbon molecular emission was used for laser-induced plasma diagnostics,[37,38] thin film preparation,[39,40] plasma fluctuations correction,[41] and as additional spectral

Received: December 5, 2012
Accepted: February 1, 2013
Published: February 1, 2013

features in LIBS applications for identifying organic materials (pathogenic bacteria, explosive residues, biological and chemical agents).[42,43] LAMIS can be implemented similar to conventional LIBS elemental analysis. For LAMIS, longer time delays after the ablation laser pulse are utilized to allow formation of molecules in the plasma from collisions of the hot atoms and ions with the ambient air. The temporal and spatial characteristics (temperature, electron density, etc) are dependent on conditions such as laser incident intensity and spot size, ambient gas composition, and pressure, and vary with axial or radial distance from the target surface. Detailed investigation of the optical emission of the plasma plume provides spatial and temporal evolution of transient species produced during ablation, such as excited atoms, ions, or molecules.[44]

Processes contributing to laser ablation, such as laser material interaction, plasma formation, plasma expansion, and collisional excitation of atoms, have been investigated in detail by a number of groups.[45−49] The formation of molecular emission in laser ablation plasmas involves a series of chemical reactions,[50] but the precise nature of their formation and the specific reactions remain relatively unknown. St-Ong et al.[51] suggested that C_2 was ablated directly from the sample due to the existence of delocalized carbon−carbon double bonds in the sample. Recently, it has been published that the recombination of carbon atoms C + C + M ↔ C_2 + M was an important process forming C_2,[52] while others argued that the most influential process in the C_2 formation was due to the reaction of C with CN and CH: CN + C ↔ C_2 + N and C + CH ↔ C_2 + H at longer delays.[53]

In this work, we used the LAMIS approach to measuring isotopic ratios with samples containing ^{12}C mixed with ^{13}C, for studying the formation of molecular C_2 and carbon isotope separation in laser ablation plasmas. A kinetic study of the plasma properties including temperature, total molecular number density, and electron density was performed to describe the influence of isotope particle motion in the plasma. Time and spatial resolved plasma analysis shows distinct regions of carbon isotope separation and mechanisms for formation of C_2.

EXPERIMENTAL SECTION

The experimental system is shown in Figure 1. An Applied Spectra RT100 system configuration was used with a Q-switched Nd:YAG laser operated at 1064 nm and 4 ns pulse-duration. Pulse energy was adjusted to 120 mJ, and the laser beam was focused using a quartz lens to a spot diameter of ∼250 μm. The fluence was 244.5 J/cm^2. The plume was imaged by two quartz lenses onto a line array fiber bundle (4.9 mm high × 0.245 mm wide), each fiber with 200 μm core diameter. The imaging ratio was ∼1.5:1. The signal on the fiber bundle was then imaged by a lens onto the entrance slit of a Czemy-Turner spectrometer (Horiba JY 1250M). The relationship between each fiber and the distance (mm) above the sample surface was calibrated by measuring the image above the sample. The height of each fiber (0.245 mm) corresponded to ∼0.38 mm height of the plasma, from the calibration. The area of each fiber image was calculated, and the emission intensity of each position (mm) was spatially averaged. Spectral emission was detected with an intensified charge-coupled device (ICCD) (Princeton Instruments, PI MAX 1024 Gen II). The detection system provides a spectral window of 7 nm and resolution of typically 0.02 nm. Temporal profiles of emission were measured by changing the detector gate delay and the gate width at the same time in order to obtain strong intensity for time and spatial analysis, but the ratio of gate width to gate delay was fixed at 0.5. The intensity was divided by the gate width to get the actual intensity as a function of distance at different gate delays.

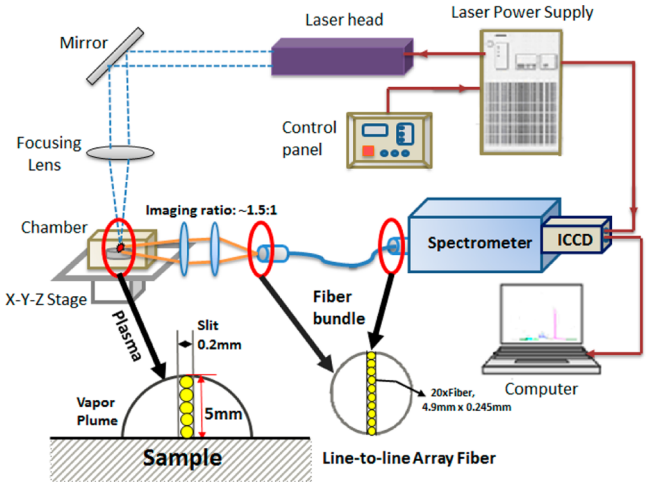

Figure 1. Experimental configuration for time and spatial imaging spectroscopy of carbon isotopes.

Benzoic acid ($C_7O_2H_6$)-^{12}C (purity ≥99.5%) and amorphous carbon-^{13}C (purity 97% and 99 atom % ^{13}C) were mixed to provide a sample with the carbon isotope ratio of $^{12}C/^{13}C$ = 2:1. The powder sample was pressed with 7 tons of pressure for 4 min into a one-centimeter diameter pellet. The sample was ablated using 10 laser shots, and one spectrum per location was obtained by accumulating consecutive laser shots. This procedure was repeated for the 6 locations on the sample in order to determine statistics of the measurements. The measurements were performed in a chamber filled with neon in order to exclude ambient air and to measure the Ne emission line (Ne I 656.3 nm) in the same spectral region close to the H line (Hα 656.287 nm). Both these elemental lines were used for the calculation of electron number density. Ne provided the highest intensity for molecular emission and the least spectral interferences, compared to measurements in Ar or He. The ablated mass was exhausted to a hood through a filter.

RESULTS AND DISCUSSION

Figure 2 shows emission for atomic and molecular carbon in a laser plasma. The C_2 molecular band exhibits large isotopic splitting compared to the small shift for the atomic emission of ^{12}C and ^{13}C, which could not be resolved using the spectrometer with 0.02 nm (Figure 2a). These data provide strong evidence that recombination plays an important role for forming C_2 in the plasma due to the presence of $^{12}C_2$, $^{12}C^{13}C$, and $^{13}C_2$ (Figure 2b) at the same time; specifically, there were no $^{12}C-^{13}C$ intermolecular bonds in the samples used here. The $\Delta\nu$ = 1 and $\Delta\nu$ = −1 isotopic bands of the C_2 Swan system ($d^3\Pi_g \rightarrow a^3\Pi_u$) were chosen in this work. We measured the $^{12}C_2$ and $^{13}C_2$ (0−0) Swan system band head shift in our previous work;[14] the shift will increase as the quantum number J increases. The shifts for $\Delta\nu$ = 1 and $\Delta\nu$ = −1 are easily measured using the 0.02 nm spectral resolution of our spectrometer; 0.77 nm for $^{13}C_2-^{12}C^{13}C$ and 0.75 nm for $^{12}C^{13}C-^{12}C_2$ were measured at the $\Delta\nu$ = 1 C_2 band head. For the $\Delta\nu$ = 1 and $\Delta\nu$ = −1 of C_2 isotopic bands, the difference is

dx.doi.org/10.1021/ac303524d | Anal. Chem. 2013, 85, 2899−2906

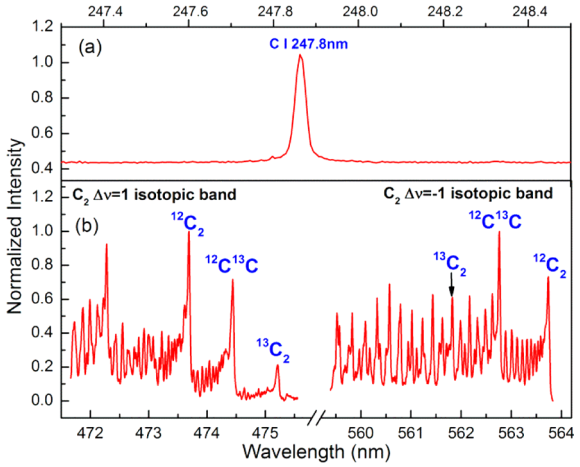

Figure 2. Emission spectra of (a) atomic carbon (b) molecular isotopic band during laser ablation of carbon isotope sample. Gate delay and width were 4 and 2 μs, respectively.

the sequence of band heads from the violet to visible. For the $\Delta\nu = 1$ C_2 isotopic band, the sequence is $^{12}C_2$, $^{12}C^{13}C$, and $^{13}C_2$ from low to high wavelength, and there is no interference from the $^{12}C_2$ and $^{12}C^{13}C$ band for $^{13}C_2$ (1−0) band head. The sequence is reversed in the $\Delta\nu = -1$ C_2 isotopic band; $^{13}C_2$ band is mixed in the band of $^{12}C_2$ and $^{12}C^{13}C$ so that it is hard to identify the $^{13}C_2$ (0−1) band head. Therefore, the $\Delta\nu = 1$ C_2 isotopic bands were chosen for these time and spatial molecular carbon emission studies. The ^{12}C and ^{13}C concentration difference in the sample results in the intensity decrease from $^{12}C_2$ through $^{12}C^{13}C$ and $^{13}C_2$ for the $\Delta\nu = 1$ C_2 isotopic bands.

Figure 3 shows the spatial evolution (emission intensity, I, versus distance, d) for C (I) atomic emission at 247.8 nm

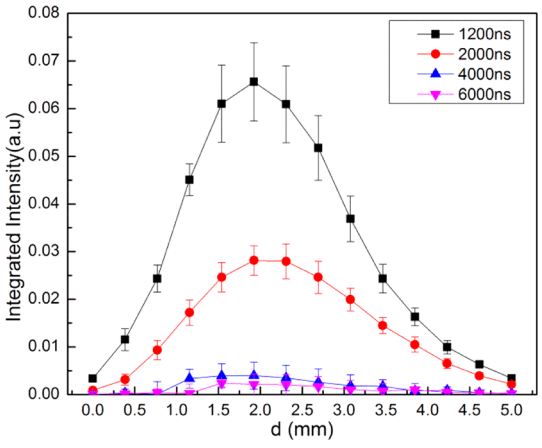

Figure 3. Spatial evolution of atomic carbon 247.8 nm emission versus gate delay.

measured versus gate delay. Data in this figure are the area of the emission line after background subtraction. The spatial evolution of isotopic molecular species ($^{12}C_2$, $^{12}C^{13}C$, and $^{13}C_2$) is plotted in Figure 4. The integrated intensity for carbon molecular spectra is derived from simulation, which will be described in detail in the molecular isotopic spectrum simulation discussion. As expected, molecular emission persists longer than that of atomic emission since it takes time for the plasma to cool and for molecular species to form. Two emission maxima versus distance were measured for $^{12}C_2$ versus gate delay up to 6000 ns, at ∼1.2 and ∼3.5 mm above the sample. The strongest peaks for $^{12}C_2$, $^{12}C^{13}C$, and $^{13}C_2$ are at ∼3.5 mm height. Only one emission peak was measured for atomic carbon at ∼2 mm above the sample. The existence of $^{12}C^{13}C$ demonstrates that recombination is a process for C_2 formation. In addition, the same maximum emission for $^{12}C_2$, $^{12}C^{13}C$, and $^{13}C_2$ at about ∼3.5 mm also suggests that recombination is a dominant process for C_2 formation.[54] The probable precursor is atomic carbon since, in the range of 2−3.5 mm, the emission intensity of C (I) decreases while C_2 emission increases. The small plateau for $^{12}C_2$ measured at lower distances suggests that fragmentation directly from the benzoic acid (^{12}C source) carbon−carbon double bonds is a viable process.[51,55,56] There are no carbon−carbon double bonds in the amorphous carbon (^{13}C source)[57] also indicating that $^{13}C_2$ also results from recombination. As the gate delay increased (after 6000 ns), the maximum emission for $^{12}C_2$, $^{12}C^{13}C$, and $^{13}C_2$ shifted from ∼3.5 to ∼2 mm and the two peaks for $^{12}C_2$ merged into one peak at ∼2 mm. As the gate delay increased, molecular temperature decreased[41] and diffusion plays an important role at later times with low temperature.[58] These processes can be addressed from the time and spatial resolved analysis of total molecular number density deduced from the simulation.

Analysis of an experimental emission spectrum with its corresponding synthetic spectrum allows us to determine appropriate parameters for the molecular bands[59,60] and also to calculate the isotope ratio. According to the Born−Oppenheimer approximation which assumes the existence of thermal equilibrium among rotational and vibrational states, the emission intensity of a molecular band ($I_{n',n'',v',v'',J',J''}$) is obtained by:[26]

$$I_{n',n'',v',v'',J',J''} = C_e \frac{q_{v',v''} S_{J',J''}}{Q_{rot} v'} (\nu_{J',J''})^4 e^{-F'hc/kT_{rot}} e^{-G'hc/kT_{vib}} \quad (1)$$

where h is Plank's constant, c is velocity of light in vacuum, k is Boltzmann's constant, and C_e is the emission constant. v and J are the vibrational and rotational quantum numbers, respectively. (v',v'') is the vibrational transition; $q_{v',v''}$ is the Franck−Condon coefficient for (v',v''), and $S_{J',J''}$ is the rotational line strengths (also known as Hönl−London factors if two states are in Hund's limiting case).[26] F' and G' are the rotational and vibrational energy terms, respectively. Q_{rot} is the rotational partition function. A detail description of diatomic molecules' spectral terms may be found in ref 26.

Our method of computing synthetic spectra is based on comparing experimentally measured intensity with calculated line intensity for each line position. The line positions are calculated on the basis of the molecular parameters. The molecular constants of $^{12}C_2$ could be found from ref 61. The molecular constants for isotopic band $^{12}C^{13}C$ and $^{13}C_2$ can be deduced according to the isotope effect such as:[26]

$$w_e^i = \rho w_e, \quad w_e^i x_e^i = \rho^2 w_e x_e, \quad B_e^i = \rho^2 B_e, \quad D_e^i = \rho^4 D_e \quad (2)$$

where w_e, $w_e x_e$, B_e, and D_e are molecular constants, $\rho = (\mu/\mu_i)^{1/2}$, μ is the reduced mass of the molecule, and i denotes the isotope. Then, the vibrational shift $\Delta\nu$ between the normal and the isotope band can be expressed as:

dx.doi.org/10.1021/ac303524d | Anal. Chem. 2013, 85, 2899−2906

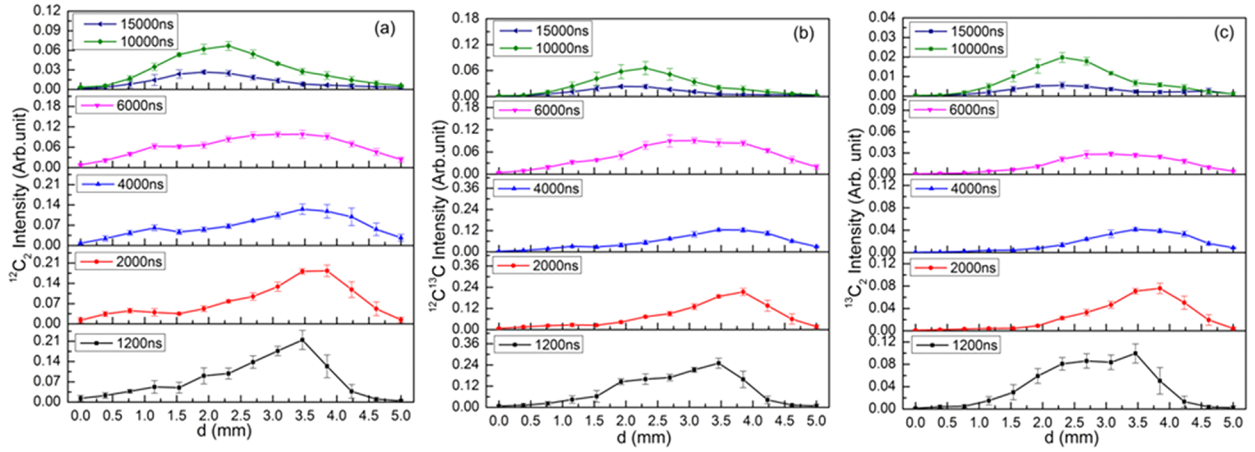

Figure 4. Spatial-evolution of integrated intensity for (a) $^{12}C_2$, (b) $^{12}C^{13}C$, and (c) $^{13}C_2$ in the range of 471.6−475.3 nm versus gate delay.

$$\Delta\nu = \nu_\nu - \nu_\nu^i = (1-\rho)\left[w_e'\left(\nu' + \frac{1}{2}\right) - w_e''\left(\nu' + \frac{1}{2}\right)\right] - (1-\rho^2)\left[w_e'x_e'\left(\nu' + \frac{1}{2}\right)^2 - w_e''x_e''\left(\nu' + \frac{1}{2}\right)^2\right] \quad (3)$$

The isotopic shift ΔF for rotational energy in diatomic molecules is:

$$\Delta F = (1-\rho^2)(F' - F'') \quad (4)$$

The transition possibilities of $^{12}C_2$, $^{12}C^{13}C$, and $^{13}C_2$ are different,[26,28] but the electronic transitions between two $^3\Pi$ states are the same. The rotational bands include P, Q, and R branches containing 9 branches. The expression of F_{vN} (with N = 1, 2, 3) for $^3\Pi-^3\Pi$ transitions could be found from ref 26. There is little isotopic effect on Franck−Condon factors which is based on the assumption that the vibrational transition probability is not affected by isotopic substitution[62] and the Franck−Condon factors for $^{12}C_2$ swan system $\Delta\nu$ = 1 sequence can be found from ref 63.

The simulation for the entire carbon isotopic band is based on the following equation:

$$I^{synth} = (N_{12C2} + N_{12C13C} + N_{13C2})[\alpha \times I_{12C2}^{synth} + \beta \times I_{12C13C}^{synth} + \gamma \times I_{13C2}^{synth}] \quad (5)$$

where N_{12C2}, N_{12C13C}, and N_{13C2} are, respectively, the molecular number densities of $^{12}C_2$, $^{12}C^{13}C$, and $^{13}C_2$. The coefficients (α, β, and γ) multiplied by the number densities (N_{12C2}, N_{12C13C}, and N_{13C2}) were proportional to the integrated intensities for $^{12}C_2$, $^{12}C^{13}C$, and $^{13}C_2$ bands, respectively, in the spectrum fitting range. Seven parameters are set as unknown: the emission constant (C_e), the rotational temperature (T_{rot}), the vibrational temperature (T_{vib}), the apparatus width ($\Delta\lambda$), and the coefficients (α, β, and γ) for $^{12}C_2$, $^{12}C^{13}C$, and $^{13}C_2$. The fitting parameters were obtained by minimizing:

$$\chi^2(T_{rot}, T_{vib}, \Delta\lambda, C_e, \alpha, \beta, \gamma) = \frac{\sum_i^N [I_i^{exp} - I_i^{synth}(T_{vib}, T_{rot}\Delta\lambda, C_e, \alpha, \beta, \gamma)]^2}{N(N-1)} \quad (6)$$

where I_i^{exp} and I_i^{synth} are the measured and calculated intensities of the i th pixel of an N point spectrum, respectively. The temperatures (T_{rot} and T_{vib}) and the coefficients (α, β, and γ) corresponding to the smallest χ^2 were taken as the appropriate fitting parameters.

Figure 5 presents experimental and computer simulated spectra for the $\Delta\nu$ = 1 sequence of the C_2 isotopic Swan band

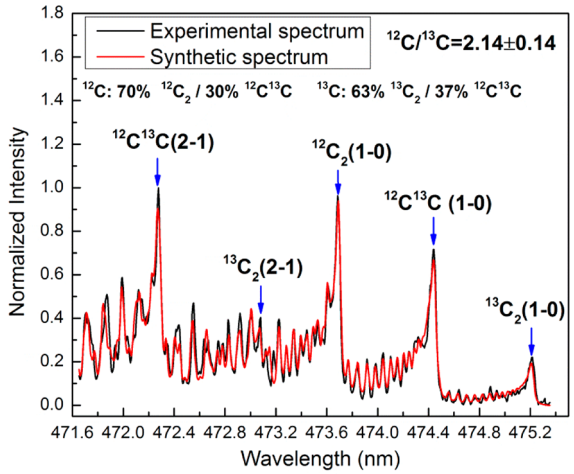

Figure 5. Experimental (black line) and simulated spectra (red line) at 3.5 mm above the sample. Gate delay and gate width were 6 and 3 μs, respectively.

in the range of 471.6−475.3 nm, which was measured at ∼3.5 mm above the sample under the gate delay and width of 6 and 3 μs; experimental and simulated spectra are in excellent agreement.

For brevity, only one gate condition (gate delay and width of 4 and 2 μs) is presented showing the vibrational and rotational temperatures as a function of height above the sample (Figure 6). Temperature of plasma dropped as the distance above the sample increased. The reason for larger error in vibrational temperature is that it mainly depends on the vibration transition (ν', ν'') and in our calculation two different vibration transitions (ν', ν'') of $\Delta\nu$ = 1 sequence − (1−0) and (2−1) bands were used for spectrum fitting. Utilizing the temperature derived from the spectrum simulation, the molecular number density can derived from eq 1 which can be expressed as:

dx.doi.org/10.1021/ac303524d | Anal. Chem. 2013, 85, 2899−2906

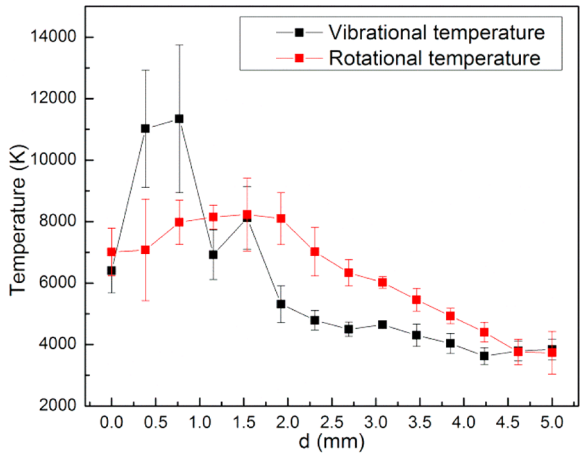

Figure 6. Vibrational and rotational temperature as a function of height above the sample. Gate delay and width were 4 and 2 μs, respectively.

$$N(T) \propto I_{C2}\cdot Q(T_{rot})/\sum_{j=0}^{N} S_{J',J''}(\nu_{J',J''})^4 e^{-F'(j)hc/kT_{rot}} e^{-G'(j)hc/kT_{vib}} \quad (7)$$

where the partition function of $^{12}C_2$ can be found from ref 64 according to the rotational temperature. The rotational partition function also can be written as:

$$Q_{rot} = \frac{kT}{\sigma hcB} \quad (8)$$

where σ = 1 for heteronuclear molecules ($^{12}C^{13}C$) and 2 for homonuclear molecules ($^{12}C_2$ and $^{13}C_2$).[65] B is the molecular constant which is related with reduced mass.[26] The spatial variation of the total molecular number density (N_{12C2} + N_{13C12C} + N_{13C2}) versus gate delay is shown in Figure 7. These

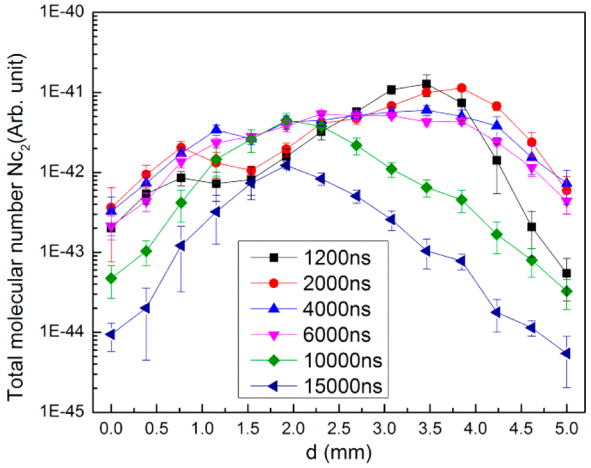

Figure 7. Spatial evolution of total molecular number densities $Nc_2(N_{12C2}+ N_{13C12C} + N_{13C2})$ versus gate delay.

data show the total molecular number relation to molecular carbon emission, and the change of observation intensity is deduced by the molecular number density. There are two distinctive peaks in the spatial distribution at gate delay up to 6 μs that later merge into one peak, and the peak maximum shifts from ~3.5 to ~2.0 mm; similar to the $^{12}C_2$ emission in Figure 4a. Diffusion and/or vortex in the plume could be a reason for the peak merging. A velocity gradient would establish a vortex ring within the vapor plume flow between the evaporated material and the stationary sample. This vortex ring provides a lift force on the vapor plume and pushes the high emission region of the vapor plume away from the sample surface.[58] As the gate delay increased, the force decreases and the peak maximum moves toward the sample surface.

Theoretical simulation also could be used to extract isotopic ratios from the molecular bands when spectral normalization was performed before spectral fitting. The isotopic ratio of $^{12}C/^{13}C$ was deduced from the coefficients (α, β, and γ) of $^{12}C_2$, $^{12}C^{13}C$, and $^{13}C_2$ as a function of distance versus gate delay (Figure 8). The violet line in the plot indicates the

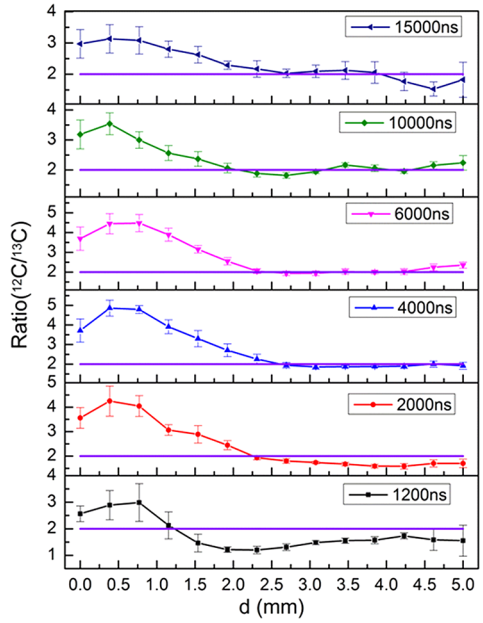

Figure 8. Isotope ratio of $^{12}C/^{13}C$ derived from the $^{12}C_2$, $^{12}C^{13}C$, and $^{13}C_2$ as a function of distance versus gate delay. The violet line indicates the nominal ratio of $^{12}C/^{13}C$ (2:1) in the sample.

nominal ratio of $^{12}C/^{13}C$ (2:1) in the sample. The ratio is greater than 2 in the range of 0–2.3 mm, indicating that there was more ^{12}C in the inner zone and more ^{13}C in the outer zone of the plasma. This phenomenon is especially obvious at early times (gate delay with 1200 and 2000 ns). As the gate delay increased, the ratio was close to the nominal ratio (2:1) in the outer zone (2.3–4.3 mm) of the plasma. These data support that carbon isotopes ($^{12}C/^{13}C$) can be separated in laser ablation plumes, and the change in ratio is related with the time and spatial distance above the sample.

To elucidate the isotope ratio ($^{12}C/^{13}C$) change versus time and height, the dynamic change in the plasma condition is addressed with regard to the fact that the plasma temperature is above 10 000 K, especially near the sample surface. Also, the assumption is made that the plume approaches local thermal equilibrium in the time interval due to collisions between electrons and atoms being much smaller than 1 μs. Carbon is almost completely decomposed to give $^{12}C^+$, $^{13}C^+$, $^{12}C_2$, $^{13}C_2$, $^{12}C^{13}C$, ^{12}C, ^{13}C and electrons e^- as the species constituting the plasma. The number densities are respectively expressed by N_1, N_2, N_3, N_4, N_5, N_6, N_7, and N_e (m^{-3}). Saha's thermal ionization equilibrium and diatomic molecular dissociation into constit-

dx.doi.org/10.1021/ac303524d | Anal. Chem. 2013, 85, 2899–2906

uent atoms (Guldberg-Waage's law)[65] can be expressed as follows:

$$\frac{N_e N_1}{N_6} = K_1(T) \quad (9)$$

$$\frac{N_e N_2}{N_7} = K_2(T) \quad (10)$$

$$\frac{N_6^2}{N_3} = K_3(T) \quad (11)$$

$$\frac{N_6 N_7}{N_5} = K_4(T) \quad (12)$$

$$\frac{N_7^2}{N_4} = K_5(T) \quad (13)$$

$$\frac{N_6 + N_1 + 2N_3 + N_5}{N_7 + N_2 + 2N_4 + N_5} = \theta \quad (14)$$

$$N_1 + N_2 + N_3 + N_4 + N_5 + N_6 + N_7 = \frac{p}{RT} \quad (15)$$

where $K_1(T)$ and $K_2(T)$ are, respectively, the equilibrium constant of monovalent carbon isotope ions $^{12}C^+$ and $^{13}C^+$; $K_3(T)$, $K_4(T)$, and $K_5(T)$ are the equilibrium constant of molecular $^{12}C_2$,$^{12}C^{13}C$, and $^{13}C_2$, respectively; p is the atmospheric pressure, and θ is the ^{12}C concentration in the ^{13}C molecule concentration (in this work, the isotopic ratio of $^{12}C/^{13}C$ was 2:1). This analysis gives seven unknowns of N_1, N_2, N_3, N_4, N_5, N_6, and N_7. T and N_e are known parameters; T is determined from the spectrum simulation and N_e could be deduced from Hα 656.287 nm Stark broadening.[66] The equilibrium constant $K(T)$ is not only related with the temperature (T) but also related with the internal energy partition. The internal partition functions of both atoms and molecule are the sums of the weighted Boltzmann factors of all levels, including the nuclear hyperfine levels. The nuclear spin values of ^{12}C and ^{13}C are 0 and 0.5, respectively;[26] thus, the atomic and ionic ^{12}C partition functions are two times smaller than that of ^{13}C. For the carbon Swan molecular spectrum, an electronic spin $S = 1$ produces the triplet structure. For the homonuclear $^{13}C_2$ molecule, the nuclear spin $I = 0.5$ causes the lines of the resolved doublet to have a 3:1 intensity ratio. For the heteronuclear $^{12}C^{13}C$ molecule, the lines of the resolved Λ-doublet have equal intensities. For the terrestrially abundant $^{12}C_2$ molecule, the nuclear spin $I = 0$ causes one line of each Λ-doublet to be missing.[26] Therefore, considering the influence of symmetry factor σ for the homonuclear molecule and the effect of nuclear spin, the ratio of internal partition function for $^{12}C_2$, $^{12}C^{13}C$, and $^{13}C_2$ is 1:4:4. According to this ratio, the partition function of all the carbon isotopic particles could be acquired from that of $^{12}C_2$ which could be found from ref 64. According to eqs 9–15, we can calculate the particle number densities for $^{12}C^+$, $^{13}C^+$, $^{12}C_2$, $^{13}C_2$, $^{12}C^{13}C$, ^{12}C, and ^{13}C. Then, the ratio of ^{12}C to ^{13}C can be derived from the number densities of $^{12}C_2$, $^{12}C^{13}C$, and $^{13}C_2$ for calculated temperatures and electron densities. Our calculated results show that the $^{12}C/^{13}C$ ratio changed little ranging from 2.00 to 2.04. Therefore, the measured ratio is not from the influence of mass action and Saha ionization processes which resulted in the change of plasma condition.

Isotope separation can be related with the inhomogeneity of laser-induced plasmas. Figure 9 shows the spatial evolution of

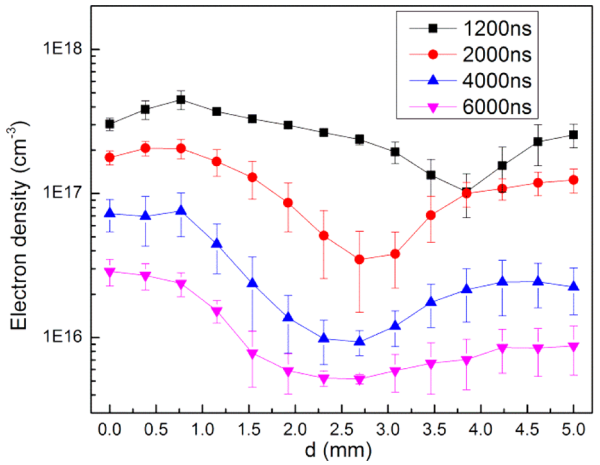

Figure 9. Spatial evolution of electron number density derived from Hα 656.287 nm at different gate delay.

electron densities versus gate delay. The electron density is greater close to the sample and is related with time and distance. The electron density increased at early times at the outer zone of plasma and the minimum electron density moved toward the surface as the gate delay was increased. Shockwave heating can produce the increased electron densities at greater distance.[67] We also studied the relationship between electron densities and the ratio of $^{12}C/^{13}C$ in the spatial range of 0.4–2.30 mm (Figure 10). This is the range where the ratio

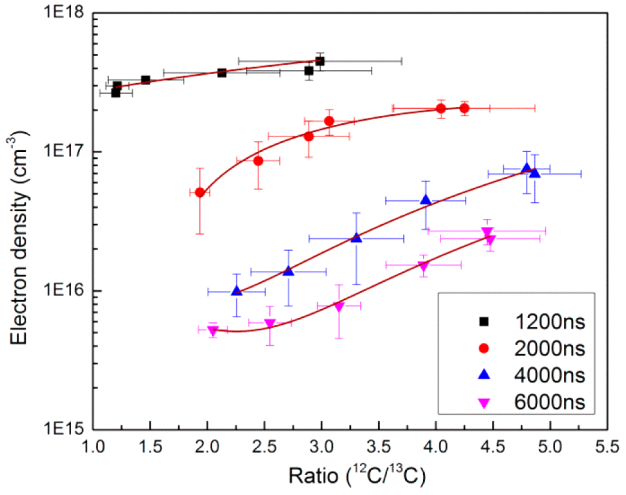

Figure 10. Relationship between electron densities and the ratio of $^{12}C/^{13}C$ in the spatial range of 0.4–2.30 mm at different gate delay. The wine lines indicate the best-fit curves of the experimental data sets.

significantly deviated from the nominal ratio of $^{12}C/^{13}C$ (2:1). There are no internal electric fields in a homogeneous neutral plasma except within the Debye length at the plasma edge. Nearly all plasmas produced in laboratories are inhomogeneous, especially in the case of laser-induced plasmas.[68] The temporal and spatial analysis of the temperature and the electron densities support inhomogeneity of our laser ablation plasma. Hora[68] used a single particle model to show that a

dx.doi.org/10.1021/ac303524d | Anal. Chem. 2013, 85, 2899–2906

nonlinear force exists in the high internal electric fields inside of the plasmas due to the inhomogeneity. The electron charge densities are the source of the electric fields, and strong electric fields can be established between the electrons and ions. The electron field direction is opposite to the ejection of the ions, which will decelerate ^{12}C more than ^{13}C and concentrate ^{12}C close to the sample. The phenomena observed from these measurements are consistent with measurements by Suen[69] who measured isotope separation in laser plumes using orthogonal time-of-flight mass spectrometry. His work showed that ^{109}Ag was spatially ahead of the ^{107}Ag at early times.

CONCLUSION

These measurements demonstrate that the LAMIS approach is valuable for studying laser-induced plasma chemistry, as well as for the detection of isotopes. Isotopic shifts in emission spectra of the $^{12}C_2$, $^{12}C^{13}C$, and $^{13}C_2$ $\Delta\nu$ = 1 molecular Swan system were measured using LAMIS on fabricated carbon isotopic samples. The measurement of $^{12}C^{13}C$ demonstrates that C_2 was formed from recombination processes as the $^{12}C-^{13}C$ intermolecular bond did not exist in the sample. The $^{12}C/^{13}C$ was measured and modeled using synthetic spectra and found to be dependent on time after the laser pulse and distance above the sample surface. The Saha equation and law of mass action were used for the calculation of particle number density in the plasma and confirm that the influence on the isotopic ratio was not from the ionization process. The higher temperature and electron density close to the sample establishes a strong electric field with opposite direction to the ejection of the ions, which is believed to be the reason why the ratio deviated from its nominal value of $^{12}C/^{13}C$ = 2:1 in the sample.

AUTHOR INFORMATION

Corresponding Author

*E-mail: rerusso@lbl.gov. Fax: +1-510-486-7303. Tel: +1-510-486-4258.

Notes

The authors declare no competing financial interest.

ACKNOWLEDGMENTS

The research was supported by the Office of Basic Energy Sciences, Chemical Science Division and the Defense Nuclear Nonproliferation Research and Development Office of the U.S. Department of Energy under contract number DE-AC02-05CH11231 at the Lawrence Berkeley National Laboratory. M.D. and J. L. also acknowledge support from National Natural Science Foundation of China (No. 51071069 and 51206055) and the State Scholarship Fund from China Scholarship Council (CSC). We acknowledge comments from Dr. George C.Y. Chan.

REFERENCES

(1) Suen, T. W.; Mao, X.; Russo, R. E. *AIP Conf. Proc.* **2010**, *1278*, 629−634.
(2) Joseph, M.; Manoravi, P. *Appl. Phys. A: Mater. Sci. Process.* **2003**, *76*, 153−156.
(3) Pietsch, W.; Petit, A.; Briand, A. *Spectrochim. Acta, Part B* **1998**, *53*, 751−761.
(4) Letokhov, V. S. *Annu. Rev. Phys. Chem.* **1977**, *28*, 133−159.
(5) Horn, I.; Rudnick, R. L.; McDonough, W. F. *Chem. Geol.* **2000**, *164*, 281−301.
(6) Pronko, P. P; VanRompay, P. A; Zhang, Z.; Nees, J. A. *Phys. Rev. Lett.* **1999**, *83*, 2596−2599.
(7) Gupta, P. D; Naik, P. A. *Phys. Rev. Lett.* **2001**, *86*, 1386−1386.
(8) VanRompay, P. A.; Zhang, Z.; Nees, J. A.; Pronko, P. P. *Proc. SPIE* **2000**, *3934*, 43−51.
(9) Kurniawan, K. H.; Kagawa, K. *Appl. Spectrosc. Rev.* **2006**, *41*, 99−130.
(10) Doucet, F. R.; Lithgow, G.; Kosierb, R.; Bouchard, P.; Sabsabi, M. *J. Anal. At. Spectrom.* **2011**, *26*, 536−541.
(11) Cremers, D. A.; Beddingfield, A.; Smithwick, R.; Chinni, R. C.; Jones, C. R.; Beardsley, B.; Karch, L. *Appl. Spectrosc.* **2012**, *66*, 250−261.
(12) Smith, C. A.; Martinez, M. A.; Veirs, D. K.; Cremers, D. A. *Spectrochim. Acta, Part B* **2002**, *57*, 929−937.
(13) Mao, X.; Bol'shakov, A. A.; Perry, D. L.; Sorkhabi, O.; Russo, R. E. *Spectrochim. Acta, Part B* **2011**, *66*, 604−609.
(14) Russo, R. E.; Bol'shakov, A. A.; Mao, X.; McKay, C. P.; Perry, D. L.; Sorkhabi, O. *Spectrochim. Acta, Part B* **2011**, *66*, 99−104.
(15) Mao, X.; Bol'shakov, A. A.; Choi, I.; McKay, C. P.; Perry, D. L.; Sorkhabi, O.; Russo, R. E. *Spectrochim. Acta, Part B* **2011**, *66*, 767−775.
(16) Bol'shakov, A. A.; Mao, X.; McKay, C. P.; Russo, R. E. *Proc. of SPIE* **2012**, *8385*, 83850C-1−83850C-7.
(17) Gouveiaa, S. E. M.; Pessenda, L. C. R.; Aravena, R.; Boulet, R.; Scheel-Ybert, R.; Bendassoli, J. A.; Ribeiro, A. S.; Freitas, H. A. *Global Planet Change* **2002**, *33*, 95−106.
(18) Thomas, K. M.; Grant, K.; Tate, K. *Fuel* **1993**, *72*, 941−947.
(19) Nardoto, G. B.; Silva, S.; Kendall, C.; Ehleringer, J. R.; Chesson, L. A.; Ferraz, E. S. B.; Moreira, M. Z.; Ometto, J. P. H. B.; Martinelli, L. A. *Am. J. Phys. Anthropol.* **2006**, *131*, 137−146.
(20) Martinelli, L. A.; Devol, A. H.; Victoria, R. L.; Richey, J. E. *Nature* **1991**, *353*, 57−59.
(21) Silverman, S. R.; Epstein, S. *AAPG Bull.* **1958**, *42*, 998−1012.
(22) Benson, S.; Lennard, C.; Maynard, P.; Roux, C. *Forensic Sci. Int.* **2006**, *157*, 1−22.
(23) Weltner, W., Jr.; Van Zee, R. J. *Chem. Rev.* **1989**, *89*, 1713−1747.
(24) Huber, K. P.; Herzberg, G. *Molecular Spectra and Molecular Structure IV. Constants of Diatomic Molecules*; Van Nostrand Reinhold: New York, 1979; Appendix IX.
(25) Ballik, E. A.; Ramsay, D. A. *Astrophys. J.* **1963**, *137*, 61−84.
(26) Herzberg, G. *Molecular Spectra and Molecular Structure: Spectra of Diatomic Molecules*, 2nd ed; Chapman and Hall: London, 1950.
(27) Pesic, D. S.; Vujisic, B. R. *J. Mol. Spectrosc.* **1983**, *l00*, 245−259.
(28) Amiot, C. *Astrophys. J., Suppl. Ser.* **1983**, *52*, 329−340.
(29) Amiot, C.; Verges, J. *Astron. Astrophys. Suppl. Ser.* **1983**, *51*, 257−265.
(30) Curtis, M. C.; Sarre, P. J. *Mol. Phys.* **1988**, *65*, 225−235.
(31) Wong, D. M.; Bol'shakov, A. A.; Russo, R. E. *Encyclopedia of Spectroscopy and Spectrometry*, 2nd ed; Academic Press: San Diego, CA, 2010; pp 1281−1287.
(32) Russo, R. E.; Suen, T. W.; Bol'shakov, A. A.; Yoo, J. H.; Sorkhabi, O.; Mao, X.; Gonzalez, J.; Oropezaa, D.; Zorba, V. *J. Anal. At. Spectrom.* **2011**, *26*, 1596−1603.
(33) Singh, J. P., Thakur, S. N., Eds. *Laser-Induced Breakdown Spectroscopy*; Elsevier: Amsterdam, Oxford, 2007.
(34) Cremers, D. A.; Radziemski, L. J. *Handbook of Laser-Induced Breakdown Spectroscopy*; J. Wiley & Sons: New York, 2006.
(35) Miziolek, A. W., Palleschi, V., Schechter, I., Eds. *Laser-Induced Breakdown Spectroscopy (LIBS), Fundamentals and Applications*, Cambridge University Press: UK, 2006.
(36) Lee, Y. I.; Song, K.; Sneddon, J. *Laser-Induced Breakdown Spectroscopy*; Nova Science Publishers: Huntington, NY, 2000.
(37) Parigger, C. G.; Guan, G.; Hornkohl, J. O. *Appl. Opt.* **2003**, *42*, 5986−5991.
(38) Parigger, C. G.; Hornkohl, J. O.; Keszler, A. M.; Nemes, L. *Appl. Opt.* **2003**, *42*, 6192−6198.
(39) Acquaviva, S.; De Giorgi, M. L. *Appl. Surf. Sci.* **2002**, *186*, 329−334.

(40) Acquaviva, S.; De Giorgi, M. L. *J. Phys. B: At. Mol. Opt. Phys.* **2002**, *35*, 795−806.
(41) Dong, M.; Mao, X.; Gonzalez, J.; Lu, J.; Russo, R. E. *J. Anal. At. Spectrom.* **2012**, *27*, 2066−2075.
(42) Diedrich, J.; Rehse, S. J.; Palchaudhuri, S. *J. Appl. Phys.* **2007**, *102*, 014702-1−014702-8.
(43) Gottfried, J. L.; De Lucia, F.C.; Munson, C. A.; Miziolek, A. W. *Spectrochim. Acta, Part B* **2007**, *62*, 1405−1411.
(44) Harilal, S. S.; Bindhu, C. V.; Issac, R. C.; Nampoori, V. P. N.; Vallabhan, C. P. G. *J. Appl. Phys.* **1997**, *82*, 2140−2146.
(45) Capitelli, M.; Casavola, A.; Colonna, G.; DeGiacomo, A. *Spectrochim. Acta, Part B* **2004**, *59*, 271−289.
(46) Lu, Q.; Mao, S.; Mao, X.; Russo, R. E. *J. Appl. Phys.* **2008**, *10*, 083301-1−083301-7.
(47) Dijk, J. V.; Kroesen, G. M. W.; Bogaerts, A. *J. Phys. D: Appl. Phys.* **2009**, *42*, 190301-1−190301-14.
(48) Vidal, F.; Laville, S.; Johnston, T.; Barthlemy, O.; Chaker, M.; Drogoff, L. B.; Margot, J.; Sabsabi, M. *Spectrochim. Acta, Part B* **2001**, *56*, 973−986.
(49) Zhigilei, L. V.; Garrison, B. J. *Appl. Phys. A: Mater. Sci. Process.* **1999**, *69*, S75−S80.
(50) Babushok, V. I.; DeLucia, F. C., Jr.; Dagdigian, P. J.; Gottfriedb, J. L.; Munsonb, C. A.; Nuscab, M. J.; Miziolekb, A. W. *Spectrochim. Acta, Part B* **2007**, *62*, 1321−1328.
(51) St-Onge, L.; Sing, R.; Bechard, S.; Sabsabi, M. *Appl. Phys. A: Mater. Sci. Process.* **1999**, *69*, S913−S916.
(52) Zelinger, Z.; Novotny, M.; Bulir, J.; Lancok, J.; Kubat, P.; Jelinek, M. *Plasma Phys.* **2003**, *43*, 426−432.
(53) Ma, Q.; Dagdigian, P. J. *Anal. Bioanal. Chem.* **2011**, *400*, 3193−3205.
(54) Iida, Y.; Yeung, E. S. *Appl. Spectrosc.* **1994**, *48*, 945−950.
(55) Grégoire, S.; Motto-Ros, V.; Ma, Q. L.; Lei, W. Q.; Wang, X. C.; Pelascini, F.; Surma, F.; Detalle, V.; Yu, J. *Spectrochim. Acta, Part B* **2012**, *74*−*75*, 31−37.
(56) Grégoire, S.; Boudinet, M.; Pelascini, F.; Surma, F.; Detalle, V.; Holl, Y. *Anal. Bioanal. Chem* **2011**, *400*, 3331−3340.
(57) Robertson, J. *Adv. Phys.* **1986**, *35*, 317−374.
(58) Wen, S. B.; Mao, X.; Greif, R.; Russo, R. E. *J. Appl. Phys.* **2006**, *100*, 053104.
(59) Acquaviva, S. *Spectrochim. Acta, Part A* **2004**, *60*, 2079−2086.
(60) Pelleriny, S.; Musiolz, K.; Motret, O.; Pokrzywka, B.; Chapellel, J. *J. Phys. D: Appl. Phys.* **1996**, *29*, 2850−2865.
(61) Tanabashi, A.; Hirao, T.; Amano, T. *Astrophys. J. Suppl. Ser.* **2007**, *169*, 472−484.
(62) Halmann, M.; Laulicht, I. *Astrophys. J. Suppl. Ser.* **1966**, *12*, 307−321.
(63) Nicholls, R. W. *Proc. Phys. Soc. A* **1956**, *69*, 741−753.
(64) Irwin, A. W. *Astrophys. J. Suppl. Ser.* **1981**, *45*, 621−633.
(65) Tatum, J. B. *Publ. Dom. Astrophys. Obs.* **1966**, *13*, 1−17.
(66) El Sherbini, A. M.; Hegazy, H.; El Sherbini, Th. M. *Spectrochim. Acta, Part B* **2006**, *61*, 532−539.
(67) Tao, Y.; Tillack, M. S.; Harilal, S. S.; Sequoia, K. L.; O'Shay, B.; Najmabadi, F. *J. Phys. D: Appl. Phys.* **2006**, *39*, 4027−4030.
(68) Hora, H. *Plasmas at high temperature and density: application and implication of laser-plasma interaction*; Springer-Verlag: Berlin Heidelberg, 1991.
(69) Suen, T. W. *A Mass Spectrometry Study of Isotope Separation in the Laser Plume*. PhD Thesis, University of California, Berkeley, CA, 2012.